Luminescence enrichment in perovskite-lanthanide composites: Complexity and complementarity

Zhuang Liu, Xian Qin*, and Xiaogang Liu*
Department of Chemistry, National University of Singapore, Singapore, Singapore
**Corresponding authors: e-mail: chmqinx@nus.edu.sg; chmlx@nus.edu.sg*

Chapter Outline

Abbreviations

CIE	commission internationale de l'éclairage
CIGS	$CuIn_{1-x}Ga_xSe_2$
CN	coordination number
DFT	density functional theory
EQE	external quantum efficiency
IPCE	incident photon to current efficiency
LEDs	light-emitting diodes
LSCs	luminescent solar concentrators
NIR	near-infrared

Handbook on the Physics and Chemistry of Rare Earths. https://doi.org/10.1016/bs.hpcre.2021.12.002

PCE photoelectric conversion efficiency
UV ultraviolet
WLED white-light emitting diode

1 Introduction

Owing to their fascinating *d-f* and *f-f* optical transitions, trivalent lanthanide ions (Ln^{3+}) have been doped into many host materials for a wide range of applications, such as lighting, volumetric display, anticounterfeiting, and radiation detection, as well as imaging-guided medical treatment [1,2]. Optical transitions within 4*f* manifolds are of particular interest to scientific and industrial communities, as their associated photoluminescence is characterized by narrow-band, fingerprint-like emission with tunable wavelengths from the ultraviolet (UV) to near-infrared (NIR) regions [3,4]. Notably, abundant ladder-like 4*f* energy levels endow lanthanide-doped materials with intriguing linear and nonlinear optical phenomena, including downshifting, quantum cutting, and anti-Stokes upconversion (Fig. 1).

Although proof-of-concept studies of luminescence in lanthanide-doped materials have been well demonstrated, practical applications demand further improvements in both emission intensity and photon conversion efficiency as the absorption cross-sections of lanthanide ions are typically small. This is attributed to the parity-forbidden nature of electric dipole 4*f*-4*f* optical transitions. By taking advantage of nonradiative resonance energy transfer, this drawback can be effectively circumvented using sensitizers with large absorption cross-sections, such as Yb^{3+} and Nd^{3+}, semiconductors, and organic molecules [5–7].

In comparison, semiconductors have outperformed lanthanide sensitizers for energy harvesting because the former features absorption cross-sections a few orders of magnitude larger than the latter [8,9]. When compared with organic sensitizers, semiconductors feature much greater photostability. Importantly, recent studies have shown that resonance energy transfer can

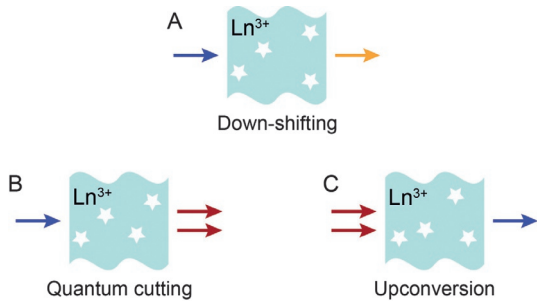

FIG. 1 Schematics of linear and nonlinear optical phenomena in lanthanide-doped luminescent materials.

occur between molecular triplet states directly to the lanthanide's 4*f* states, rather than molecular singlet states [10,11]. As such, the overall sensitization efficiency equals the product of singlet-triplet intersystem-crossing efficiency and triplet-lanthanide energy transfer efficiency. An extra step of intersystem crossing could decrease sensitization efficiency. Additionally, the bandgap emission of semiconductors can be fine-tuned to match the absorption spectral range of lanthanide ions by varying the size, shape, composition, and crystal structure of the semiconductors, or through surface modification [12]. Despite enormous research, doping of trivalent lanthanide ions into conventional semiconductors remains challenging because of ionic size mismatch and low coordination numbers typically associated with semiconductor elements [13,14].

Lead-based inorganic halide perovskites $CsPbX_3$ (X = Cl, Br, or I) have been at the forefront of scientific research, largely due to their tunable bandgaps, large absorption cross-sections, and high photoluminescence quantum yields [15–19]. Given the increase in coordination number and structural tunability, perovskite semiconductors have shown great utility in coupling lanthanide ions for light harvesting and luminescence manipulation [20–22]. For example, sensitized NIR emission has reportedly reached a quantum yield of over 190% in Yb^{3+}-doped perovskite thin films [23], which is significantly higher than that achieved in Yb^{3+}-doped CdSe, $NaInS_2$ and $PbInS_4$ nanocrystals [24,25]. In this respect, lanthanide-doped perovskites are promising for optoelectronic applications in photovoltaic modules, luminescent solar concentrators (LSCs) and light-emitting diodes (LEDs) [20,21].

In this chapter, we summarize recent advances in the development of lanthanide-doped luminescent perovskites. Emphasis is placed on mechanistic studies of energy transfer-governed sensitization and quantum cutting, followed by an overview on the recent use of these luminophores for optoelectronic performance enhancement. This chapter ends with an outlook that discusses current challenges and future promises in developing lanthanide-doped perovskite materials.

2 Lanthanide-doped lead-based inorganic halide perovskites

2.1 Lanthanide doping

Lanthanide-doped semiconductors have long been desired for linear and nonlinear optical applications [9,26,27]. Compared with ionic hosts such as fluorides and oxides, it is much more difficult to incorporate lanthanide ions into conventional semiconductors, such as silicon, II-VI, and III-V semiconductors. This can be mainly ascribed to the low coordination numbers of cation sites and the large mismatch in the ionic radii of lanthanide dopants and host cations (Fig. 2). Incompatibility in dopant-host oxidation states is another factor determining lanthanide solubility because aliovalent doping requires the

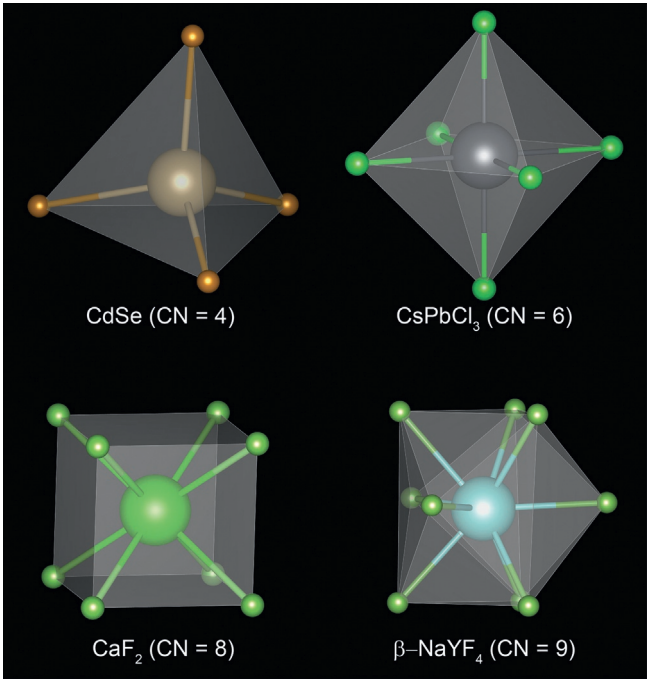

FIG. 2 Atomic illustrations of the first-coordination polyhedra of trivalent lanthanide ions doped in four different crystals.

formation of defects to maintain charge neutrality. Additionally, intrinsic host lattice defects can affect lanthanide solubility, especially in colloidal nanocrystals synthesized under thermal nonequilibrium conditions. Consequently, doping is most likely a kinetic process involving ion adsorption, diffusion, and substitution, which is greatly affected by structural defects.

Inorganic lead halide perovskites are an emerging class of semiconductors that can tolerate lattice imperfection to a large extent, as evidenced by trivial changes in their electronic structures [28]. Goldschmidt's tolerance factor (t) has been used extensively to predict the stability of the perovskite structure [29]:

$$t = (r_A + r_X)/\sqrt{2}(r_B + r_X) \tag{1}$$

where r_i (i = A, B, or X) denotes the radius of a given ion in ABX_3 perovskites. The calculated tolerance factors of $CsPbX_3$ crystals fall within the range between 0.81 and 1.11 [30], suggesting a high tolerance for lattice defects. Moreover, the octahedral index μ [31]:

$$\mu = r_B/r_X \tag{2}$$

is in the range between 0.41 and 0.90, indicating a large degree of octahedron distortion and a high probability of multiphase coexistence. Taken together, one would expect easy lanthanide doping into perovskite hosts without compromising lattice integrity.

As for $CsPbX_3$ crystals, Cs^+ and Pb^{2+} cations are bonded to 12 and 6 anions, respectively. The corresponding Shannon ionic radii for Cs^+ and Pb^{2+} ions are 188 and 119 pm, respectively, while the ionic radii of 6-coordinated Ln^{3+} fall within the range of 86–103 pm. Given the small differences in ionic radius and valency between Pb^{2+} and Ln^{3+} ions, lanthanide ions are expected to substitute Pb^{2+} ions with an octahedral coordination environment, accompanied by the formation of lattice defects for charge compensation. Such a hypothesis has been supported by experimental characterizations and quantum calculations [32,33]. Specifically, the extended X-ray absorption fine structure spectra of Yb L_{III}-edge showed that bond lengths between Yb^{3+} dopants and their neighboring Cl^- ions are close to Pb—Cl bond length, suggesting that Pb^{2+} are substituted by Yb^{3+} [33]. Moreover, similar photoluminescence decay kinetics of band-edge emission in both Yb^{3+}- and La^{3+}-doped $CsPbCl_3$ nanocrystals indicate a general replacement of Ln^{3+} for Pb^{2+}. This conclusion is consistent with density functional theory (DFT)-based first-principles calculations in which lanthanide doping at Pb^{2+} sites possesses the lowest formation energy compared with Cs^+ substitution or Ln^{3+} interstitial, irrespective of Pb chemical potentials [32,34].

Despite successful incorporation, the molar concentrations of lanthanide ions (e.g., Yb^{3+}, Er^{3+}, Ce^{3+}, and Pr^{3+}) are typically less than 10%, which is one order of magnitude lower than the nominal concentrations of starting materials. Importantly, further incorporation of lanthanides can compromise the crystallinity of perovskite nanocrystals [35]. This arises because lanthanide doping typically results in a concomitant formation of lattice defects such as Pb^{2+} vacancies. Although halogen vacancies can assist lanthanide doping, the reported Yb^{3+} concentration in $CsPbCl_3$ nanocrystals synthesized under chloride-deficient conditions remains low (3.04%) [33].

2.2 Optical features of lanthanide-doped lead inorganic halide perovskites

Alloying perovskites with different lanthanide ions enables tunable emission wavelengths from visible to NIR-II [32,36]. Optical characterizations reveal that lanthanide doping slightly shifts exciton emission to higher energy as the atomic number of lanthanide dopants increases, while photoluminescence profiles of Ln^{3+} maintain characteristic *4f-4f* transition patterns (Fig. 3). Importantly, lanthanide doping enhances overall nanocrystal emission, which can be ascribed to enhanced lanthanide emission by host sensitization, as manifested by decoupled quantum yields (Fig. 4). As the doping concentration

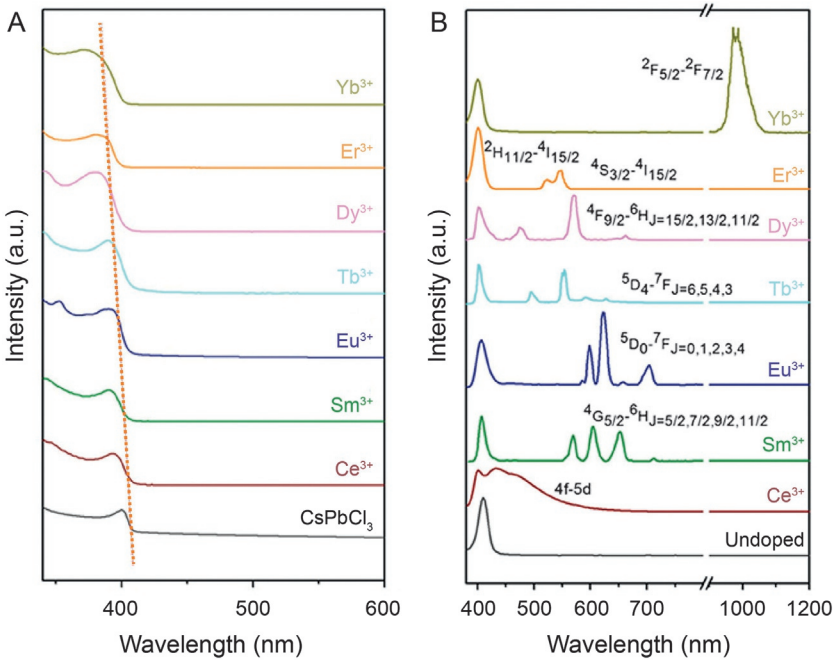

FIG. 3 (A) Absorption and (B) emission spectra of Ln^{3+}-doped and pristine $CsPbCl_3$ nanocrystals. *Adapted with permission from G. Pan, X. Bai, D. Yang, X. Chen, P. Jing, S. Qu, L. Zhang, D. Zhou, J. Zhu, W. Xu, B. Dong, H. Song, Doping lanthanide into perovskite nanocrystals: highly improved and expanded optical properties, Nano Lett. 17 (2017) 8005–8011, 10.1021/acs.nanolett.7b04575 © 2017 American Chemical Society.*

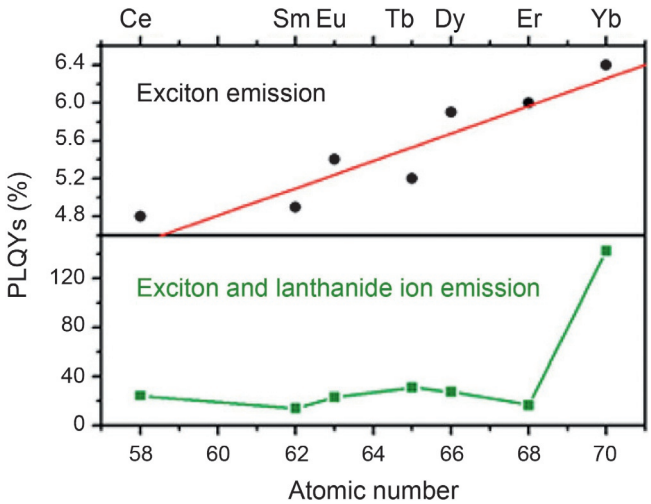

FIG. 4 Overall and projected photoluminescence quantum yields of Ln^{3+}-doped and pristine $CsPbCl_3$ nanocrystals. *Adapted with permission from G. Pan, X. Bai, D. Yang, X. Chen, P. Jing, S. Qu, L. Zhang, D. Zhou, J. Zhu, W. Xu, B. Dong, H. Song, Doping lanthanide into perovskite nanocrystals: highly improved and expanded optical properties, Nano Lett. 17 (2017) 8005–8011, 10.1021/acs.nanolett.7b04575 © 2017 American Chemical Society.*

increases, the quantum yield of exciton emission first increases and then decreases, suggesting that low-concentration doping suppresses defect-induced nonradiative recombination [37,38]. However, the nature of doping-induced enhancement in exciton emission remains unclear. Lanthanide doping may increase the formation energies of defects, leading to a reduced number of deep traps and thus alleviated nonradiative decays. On the other hand, suppression of nonradiative decay may originate from doping-induced shallow traps that may effectively compete with deep traps [39]. Consequently, charge carriers in shallow traps escape back to the host band edge for radiative recombination, resulting in increased exciton quantum yields.

Another exciting discovery is that the quantum yield of NIR emission from Yb^{3+} dopants in perovskites can exceed 100% (Fig. 4), indicative of a nonlinear quantum-cutting phenomenon. For example, quantum yields of 193% and 183% have been reported in Yb^{3+}-doped $CsPb(Cl_xBr_{1-x})_3$ thin films that are prepared by spin-coating [23] and single-source vapor deposition [40], respectively. Such high quantum yields are comparable to those observed in their nano-sized counterparts [39,41]. Although quantum cutting with high quantum yields has been reported in inorganic crystals doped with Tb^{3+}-Yb^{3+}, Tm^{3+}-Yb^{3+}, and Pr^{3+}-Yb^{3+} pairs, hybrid lanthanide-perovskite systems exhibit more efficient quantum cutting than lanthanides alone because of the large absorption cross-sections of perovskites [42]. Additionally, single-crystal and nanocrystal samples showed similar spectral and photophysical characteristics, suggesting that quantum cutting is an intrinsic property of Yb^{3+}-doped perovskites (Fig. 5) [43].

Apart from singly doping, codoping of different lanthanide ions is also feasible in perovskites to impart new optical features and enhance quantum yields. When codoped with Yb^{3+} and Er^{3+}, the NIR emission of Er^{3+} was detected in $CsPbCl_3$ nanocrystals [44–46]. The excitation spectra of $CsPbCl_3$:Yb/Er nanocrystals suggested that the perovskite host sensitizes Yb^{3+} instead of Er^{3+} because the monitored 1540-nm emission of Er^{3+} is not responsive to the 280–400 nm UV excitation (Fig. 6). Additionally, multi-color emission has been achieved in a specific class of perovskite nanophosphors codoped with Yb^{3+} and Mn^{2+} [47]. By varying the doping concentration, intensity ratios between exciton, Mn^{2+}, and Yb^{3+} emissions change accordingly, giving rise to different emission colors (Fig. 7A). This effect is attributable to the host-Mn^{2+}, host-Yb^{3+}, and Mn^{2+}-Yb^{3+} energy transfer, as corroborated by concentration-dependent photoluminescence decay measurements (Fig. 7B and C).

Codoping of optically inert species into perovskites represents another useful approach to tailoring optical properties. For instance, bright blue-violet emission with 36.5% quantum yield was obtained in $CsPbCl_3$ quantum dots after cooping of non-emissive F^- and La^{3+} ions [48]. This quantum yield is one order of magnitude higher than that of nondoped samples. Other examples include Sm^{3+}-doped $CsPbCl_3$ nanocrystals that show high-efficiency electroluminescence with tunable emission colors [49]. The maximal quantum yield

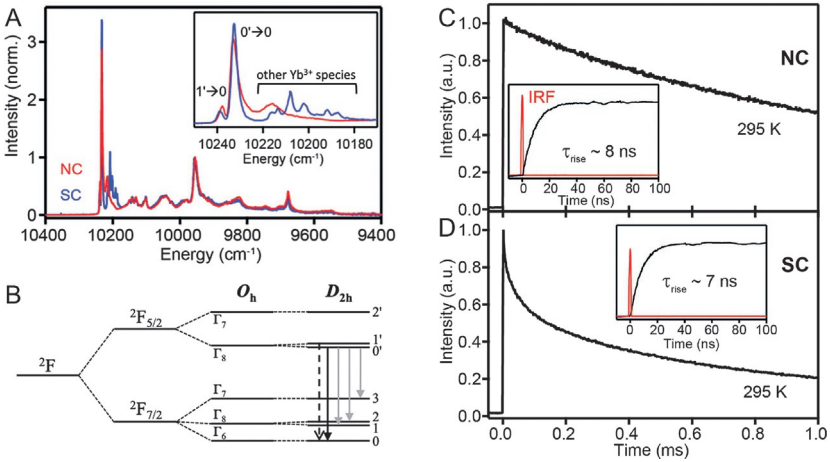

FIG. 5 (A) Photoluminescence spectra of $CsPbCl_3:Yb^{3+}$ nanocrystals and single crystals, measured at 5 K and normalized to the peak at ~9960 cm^{-1}. The inset is the enlarged view of peaks within the energy range between 10,230 and 10,170 cm^{-1}. (B) Schematics showing the crystal-field splitting of 4*f* energy levels of Yb^{3+}. (C and D) Room-temperature time-resolved photoluminescence data of $CsPbCl_3:Yb^{3+}$ nanocrystals and single crystals, respectively. The insets show the first 100 ns of the time-resolved photoluminescence trace. IRF denotes instrument response function. $\lambda_{ex} = 404$ nm, and $\lambda_{em} = 985$ nm. *Adapted with permission from J.Y.D. Roh, M.D. Smith, M.J. Crane, D. Biner, T.J. Milstein, K.W. Krämer, D.R. Gamelin, Yb^{3+} speciation and energy-transfer dynamics in quantum-cutting Yb^{3+}-doped CsPbCl3 perovskite nanocrystals and single crystals, Phys. Rev. Mater. 4 (2020) 105405, 10.1103/PhysRevMaterials.4.105405 © 2020 American Physical Society.*

(85%) was observed for 10% Sm^{3+}-doped samples. As an added benefit, the incorporation of Sm^{3+} enhances the chemical stability of perovskite nanocrystals, which can be attributed to surface passivation by lanthanide ions.

2.3 Energy transfer and quantum cutting

When employing perovskites as sensitizers, energy transfer efficiency from perovskite hosts to lanthanide emitters essentially determines the ultimate luminescence intensity and quantum yield of doped phosphors, which bears resemblance to lanthanide sensitizer-activator pairs (e.g., Yb^{3+}-Er^{3+}). Let's take energy transfer in Yb^{3+}-doped $CsPb(Cl_xBr_{1-x})_3$ nanocrystals for illustration [39]. Upon 365-nm irradiation, pristine perovskite hosts exhibit sharp exciton emission at 410 nm (Fig. 8A). Following lanthanide doping, exciton emission from $CsPbCl_3$ nanocrystals decreases dramatically, while an intense emission from Yb^{3+} at 990 nm emerges, suggesting efficient energy transfer from the perovskite matrix to Yb^{3+} (Fig. 8B). Moreover, the NIR emission intensity increases with increased Yb^{3+} concentration (Fig. 8C), indicating that cross-relaxation and surface-related quenching are trivial in these nanocrystals.

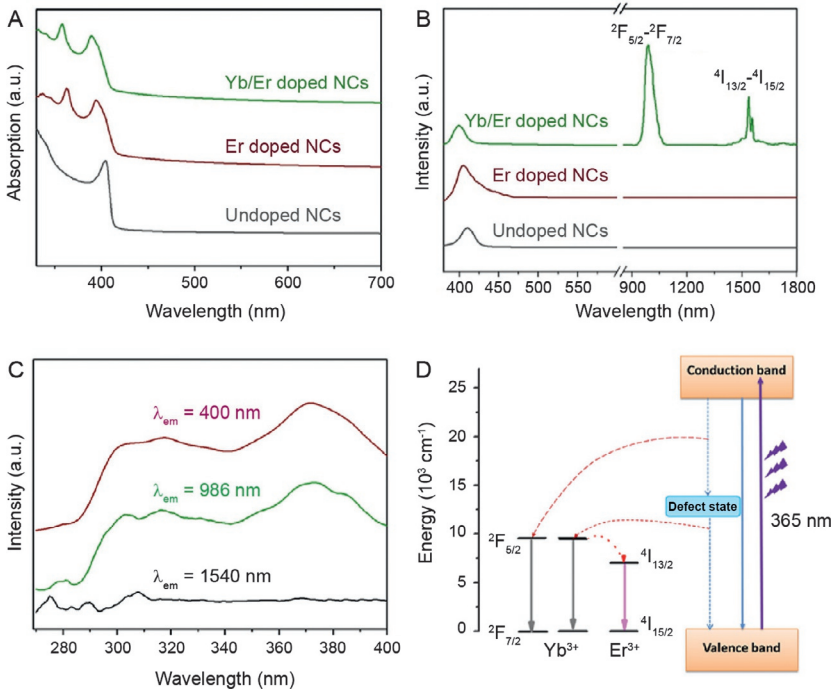

FIG. 6 (A) Absorption spectra of $CsPbCl_3$, $CsPbCl_3$:Er, and $CsPbCl_3$:Yb/Er nanocrystals. (B) Emission spectra of $CsPbCl_3$, $CsPbCl_3$:Er, and $CsPbCl_3$:Yb/Er nanocrystals under 365-nm excitation. (C) Excitation spectra of $CsPbCl_3$:Yb/Er nanocrystals monitored at 400, 986, and 1540 nm. (D) Schematic of energy transfer in $CsPbCl_3$:Yb/Er nanocrystals. *Adapted with permission from Y. Zhu, G. Pan, L. Shao, G. Yang, X. Xu, J. Zhao, Y. Mao, Effective infrared emission of erbium ions doped inorganic lead halide perovskite quantum dots by sensitization of ytterbium ions, J. Alloys Compd. 835 (2020) 155390, 10.1016/j.jallcom.2020.155390 © 2020 Elsevier Science B.V.*

Time-resolved photoluminescence characterization revealed fast host-to-Yb^{3+} energy transfer at a picosecond timescale, leading to enhanced photoluminescence intensity and quantum yield (Fig. 8D).

Energy transfer in Sm^{3+}- and Eu^{3+}-doped $CsPbCl_3$ nanocrystals closely resembles that in Yb^{3+}-doped counterparts [49,50]. Under 365-nm illumination, electrons can be excited from the valence band to the conduction band of the perovskite host, generating electron-hole pairs in the host. The Coulomb attraction triggers electron-hole recombination, followed by exciton emission. In the presence of lanthanide dopants, energy transfer from excitons to lanthanides dominates, populating the excited states of lanthanides. Subsequent depopulation leads to spontaneous lanthanide emission. Of note, phonon may participate in both host-to-lanthanide energy transfer and nonradiative decay between closely lying energy levels of lanthanide emitters.

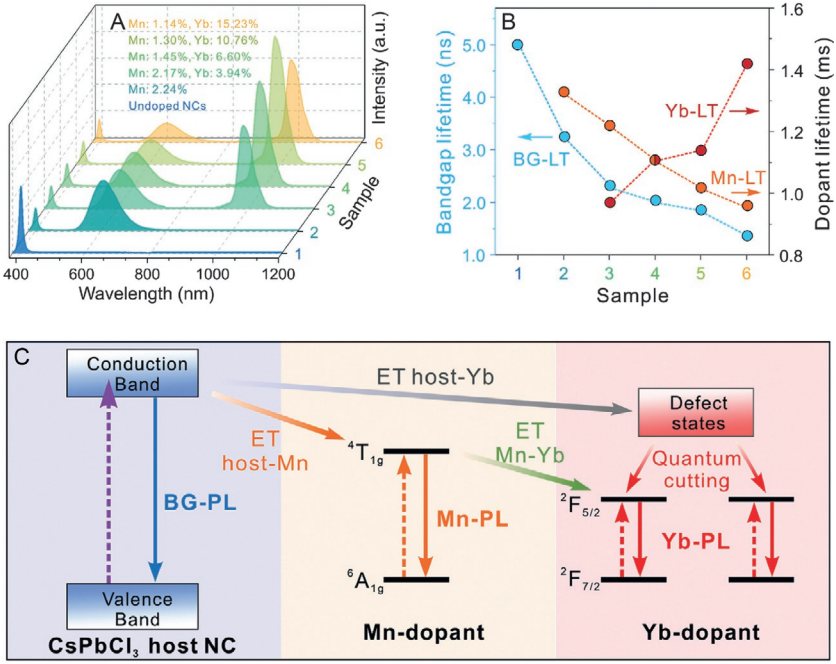

FIG. 7 (A) Photoluminescence spectra of undoped and Mn/Yb-codoped $CsPbCl_3$ nanocrystals. (B) Compiled average lifetimes for exciton, Mn^{2+}, and Yb^{3+} photoluminescence. (C) Schematic of energy transfer in $CsPbCl_3$:Mn/Yb nanocrystals. *Adapted with permission from T. Cai, J. Wang, W. Li, K. Hills-Kimball, H. Yang, Y. Nagaoka, Y. Yuan, R. Zia, O. Chen, Mn^{2+}/Yb^{3+} codoped $CsPbCl_3$ perovskite nanocrystals with triple-wavelength emission for luminescent solar concentrators, Adv. Sci. 7 (2020) 2001317, 10.1002/advs.202001317 © 2020 John Wiley and Sons.*

Fast, efficient energy transfer also endows Yb-doped perovskites with NIR emission over 100% quantum yield. This indicates that one exciton is converted into two NIR photons, a nonlinear optical phenomenon known as quantum cutting. In principle, a prerequisite for quantum cutting luminescence is that the excitation photon must have energy higher than the sum of the two or more emitted photons. Given that the total energy of two emitted NIR photons from Yb^{3+} at a low temperature is 2.53 eV, quantum cutting occurs only under excitation above this threshold (ca. 490 nm) [51]. By changing the anion composition, perovskite nanocrystals with mixed chlorine and bromine can display tunable bandgaps from 3.06 eV (405 nm) in the case of $CsPbCl_3$ nanocrystals to 2.53 eV (490 nm) in the case of $CsPb(Cl_{0.25}Br_{0.75})_3$ nanocrystals. Indeed, measured photoluminescence intensity from Yb^{3+} dampens when exciton emission energy is lower than 2.53 eV (Fig. 9). The NIR emission intensity becomes zero as exciton emission energy is below 2.4 eV, suggesting termination of host sensitization.

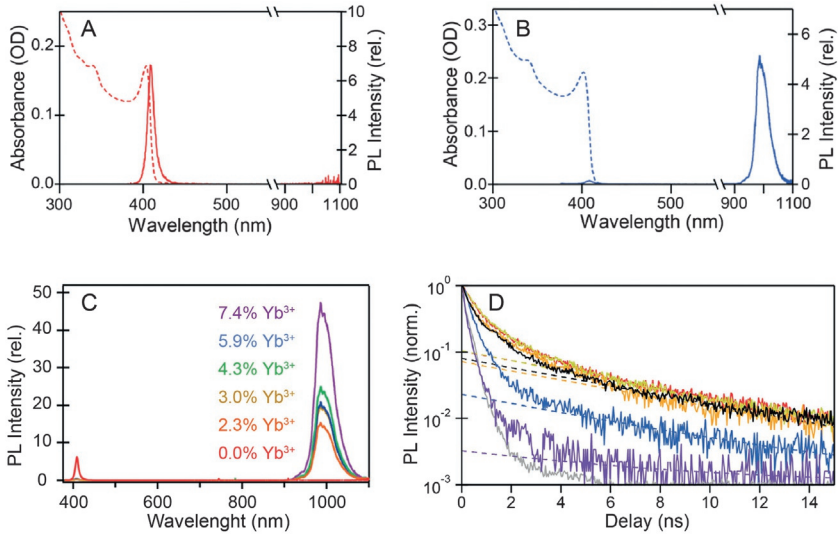

FIG. 8 (A and B) Absorption and photoluminescence spectra of nondoped and Yb^{3+}-doped $CsPbCl_3$ nanocrystals. (C) Room-temperature photoluminescence spectra of Yb^{3+}-doped $CsPbCl_3$ nanocrystals with different Yb^{3+} doping concentrations. (D) Room-temperature time-resolved photoluminescence decays of nondoped (black trace) and Yb^{3+}-doped (red to purple) $CsPbCl_3$ nanocrystals. The instrument response function is plotted in gray and shifted downward by 10^{-3} for clarity of the logarithmic presentation. *Adapted with permission from T.J. Milstein, D.M. Kroupa, D.R. Gamelin, Picosecond quantum cutting generates photoluminescence quantum yields over 100% in ytterbium-doped $CsPbCl_3$ nanocrystals, Nano Lett. 18 (2018) 3792–3799, 10.1021/acs.nanolett.8b01066 © 2018 American Chemical Society.*

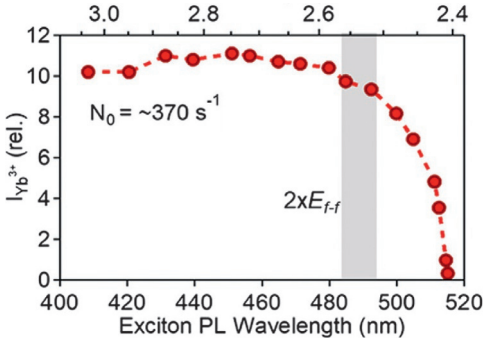

FIG. 9 Photoluminescence intensity of Yb^{3+} vs exciton photoluminescence wavelength. The gray area denotes the energy threshold for quantum cutting in $CsPb(Cl_{0.25}Br_{0.75})_3$ nanocrystals; N_0 is the constant excitation rate per nanocrystal in photons per second. *Adapted with permission from T.J. Milstein, K.T. Kluherz, D.M. Kroupa, C.S. Erickson, J.J. De Yoreo, D.R. Gamelin, Anion exchange and the quantum-cutting energy threshold in ytterbium-doped $CsPb(Cl_{1-x}Br_x)_3$ perovskite nanocrystals, Nano Lett. 19 (2019) 1931–1937, 10.1021/acs.nanolett.8b05104 © 2019 American Chemical Society.*

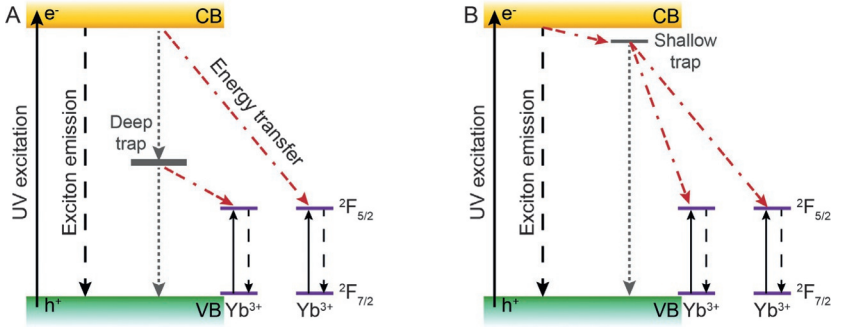

FIG. 10 Schematics of quantum-cutting mechanisms. Solid, dashed, dotted, and dash-dotted lines denote photon absorption, radiative recombination, nonradiative decay, and nonradiative resonance energy transfer, respectively. h^+: holes; e^-: electrons; CB: conduction band; VB: valence band.

Two mechanisms have been proposed to explain quantum cutting in Yb^{3+}-doped perovskites. One argument is that energy transfer from the host to Yb^{3+} is a stepwise process, in which excitation energy is separated into two portions by defect-induced deep trap states and transferred to two neighboring Yb^{3+} ions (Fig. 10A) [32,44,46]. Another mechanism claims that Yb^{3+} doping-induced shallow traps depopulate host excitons within hundreds of femtoseconds and transfer energy to two neighboring Yb^{3+} emitters simultaneously on picosecond time scales (Fig. 10B) [23,39,52]. Low-temperature shallow-trap emission has also been reported from $CsPbCl_3$ single crystals and nanocrystals doped with optically inactive La^{3+} ions, suggesting that doping-induced shallow traps are associated with interior lattice defects rather than surface-related defects [39,53]. Importantly, fast energy transfer from $CsPbCl_3$ hosts to lanthanide ions can compete with exciton recombination and remain highly efficient even at cryogenic temperatures.

The general consensus is that aliovalent doping requires formation of charge-compensating defects. For lanthanide-doped perovskites, a Yb^{3+}-V_{Pb}-Yb^{3+} cluster, analogous to the "Mcpherson pairs" in $CsCdBr_3$ doped with trivalent cations, has been proposed as the origin of those shallow traps [54]. DFT calculations reveal that a right-angle Yb^{3+}-V_{Pb}-Yb^{3+} cluster with the least formation energy is most likely to form compared with other configurations (Fig. 11) [55]. Considering that such charge-neutral defects do not introduce any mid-gap states, deep-trap-mediated stepwise sensitization of two Yb^{3+} ions is unlikely to occur, whereas simultaneous sensitization of two Yb^{3+} favors quantum cutting. However, the depopulation of host excitons via shallow traps is not supported by DFT calculations. This discrepancy arises because Pb vacancies only introduce shallow traps within the valence band rather than below the conduction band. These traps have a trivial influence on optical properties of halide perovskites, consistent with the fact that perovskites have high defect tolerance [56,57]. Instead, DFT calculations

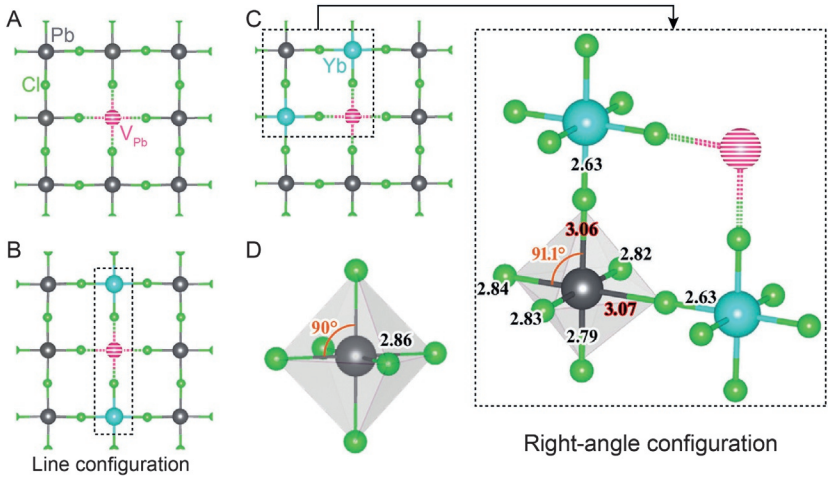

FIG. 11 (A) Atomic structure of $CsPbCl_3$ with a Pb vacancy. (B and C) Atomic structures of Yb-doped $CsPbCl_3$ with a Yb^{3+}–V_{Pb}–Yb^{3+} cluster in line and right-angle configurations, respectively. (D) Atomic scheme of a $PbCl_6$ octahedron in pristine $CsPbCl_3$ crystals. *Adapted with permission from X. Li, S. Duan, H. Liu, G. Chen, Y. Luo, H. Ågren, Mechanism for the extremely efficient sensitization of Yb^{3+} luminescence in $CsPbCl_3$ nanocrystals, J. Phys. Chem. Lett. 10 (2019) 487–492, 10.1021/acs.jpclett.8b03406 © 2019 American Chemical Society.*

suggest that the right-angle defects increase the density of electronic wave function of adjacent Pb atoms and facilitate tapping of host excitons for quantum cutting.

2.4 Photoluminescence saturation

Yb^{3+}-doped quantum cutters suffer from luminescence saturation under moderate excitation density. As a case in point, Yb^{3+}-doped perovskite thin-film yields 193% NIR emission at a power density of $\sim 10^{13}\,cm^{-2}\,s^{-1}$ and below 50% at an excitation fluence of $\sim 10^{16}\,cm^{-2}\,s^{-1}$ upon 375-nm irradiation (Fig. 12) [23]. This photon flux is equivalent to that under AM1.5 solar irradiation, necessitating new strategies to mitigating luminescence saturation in practical applications. Mechanistic studies indicate that the microscopic origin of power saturation is likely the large absorption cross-section of the perovskite host and the long excited state lifetimes of Yb^{3+}, leading to two nonradiative deactivation mechanisms [52]. Simulations of saturation behavior using a kinetic model reveal that Auger-type cross-relaxation between photoexcited hosts and pre-excited Yb^{3+} resembles experimental observation. Specifically, Yb^{3+} ions that have undergone first-round excitonic excitation can be excited to the lowest halide-to-metal charge-transfer state upon second-round excitonic excitation. Ensuing nonradiative relaxation to the $^2F_{5/2}$ state of Yb^{3+} results in decreased quantum yield (Fig. 13).

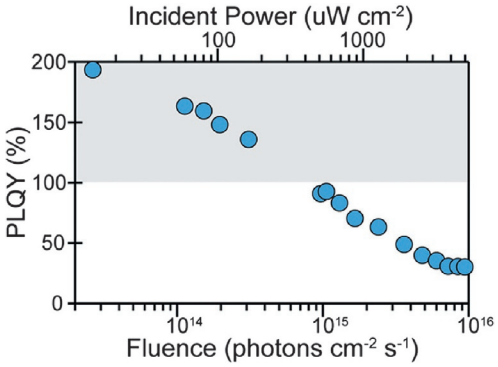

FIG. 12 Fluence dependence of the Yb^{3+} NIR quantum yield of a $CsPb(Cl_{0.35}Br_{0.65})_3$:Yb thin film measured upon 375-nm excitation. *Adapted with permission from D.M. Kroupa, J.Y. Roh, T.J. Milstein, S.E. Creutz, D.R. Gamelin, Quantum-cutting ytterbium-doped $CsPb(Cl_{1-x}Br_x)_3$ perovskite thin films with photoluminescence quantum yields over 190%, ACS Energy Lett. 3 (2018) 2390–2395, 10.1021/acsenergylett.8b01528 © 2018 American Chemical Society.*

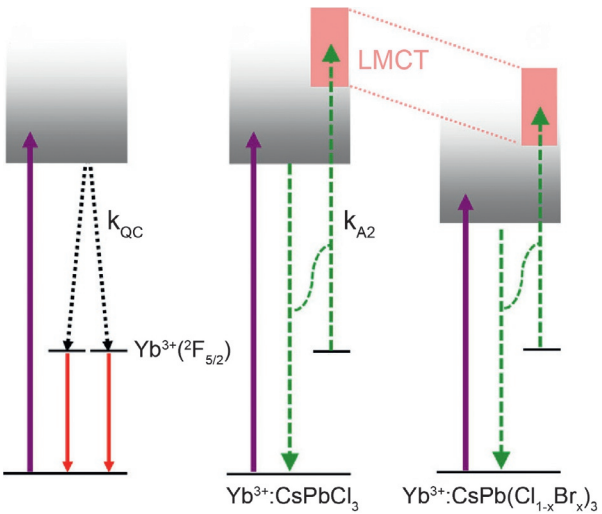

FIG. 13 Schematic showing the underlying mechanism of photoluminescence saturation in quantum-cutting Yb-doped perovskites. *Adapted with permission from C.S. Erickson, M.J. Crane, T.J. Milstein, D.R. Gamelin, Photoluminescence saturation in quantum-cutting Yb^{3+}-doped $CsPb(Cl_{1-x}Br_x)_3$ perovskite nanocrystals: implications for solar downconversion, J. Phys. Chem. C 123 (2019) 12474–12484, 10.1021/acs.jpcc.9b01296 © 2019 American Chemical Society.*

Based on the proposed mechanism, power saturation could be suppressed by decreasing the photoexcitation rate of each Yb^{3+} ion, shortening the lifetime of Yb^{3+} ions, or suppressing Auger-type cross-relaxation [52]. The first approach has proven effective because power saturation becomes less

prominent with increased Yb^{3+} concentration. It should be noted that reduced saturation may come at the cost of energy-migration-induced luminescence quenching [58]. To deactivate Yb^{3+} excited states, incorporating plasmonic structure into lanthanide-doped perovskites could be an effective strategy because plasmon-photon interaction enlarges the electromagnetic local density of states via the Purcell effect, greatly enhancing spontaneous emission rate [59]. Considering that plasmonic structures can introduce nonradiative decay channels, interactions between plasmons, excitons, and NIR photons deserve further investigation in order to alleviate power saturation, while retaining high quantum cutting efficiency [60]. The most straightforward method to suppress nonradiative cross-relaxation is to change the energy gap between the $^2F_{5/2}$ and halide-to-metal charge-transfer states of Yb^{3+}. Nonradiative resonance energy transfer from the host to pre-excited Yb^{3+} ions is likely inefficient due to a spectral mismatch.

3 Optoelectronic applications

3.1 Solar photovoltaics

Thermalization losses have placed severe constraints on the conversion efficiency of single-junction solar photovoltaics. Although above-band-gap energies can be utilized in tandem or multi-junction photovoltaics, construction of these photovoltaics requires current matching, interface engineering, and additional hardware, inevitably increasing manufacturing costs. An alternative is to integrate single-junction solar modules with down-shifting materials that are capable of efficiently converting above-band-edge photons into near-band-edge photons. By virtue of all-optical wavelength conversion, the complex fabrication of integrated solar photovoltaics can be effectively circumvented.

Owing to their high conversion efficiency, quantum cutters hold promise in enhancing solar power conversion efficiency. Theoretical calculations show that the integration of an ideal photovoltaic module with an ideal quantum cutter can achieve 40% conversion efficiency [61]. Among those reported quantum cutters, Yb^{3+}-doped perovskites are characterized by large blue/UV absorption cross-sections and high NIR emission efficiencies, making them particularly suitable as photon converters in combating thermalization losses. Additionally, quantum cutting in Yb^{3+}-doped perovskites is an intrinsic phenomenon [43], suggesting that these materials can be prepared in the form of either nanocrystals or single-crystal thin-films for ease of integration.

The first proof-of-concept fabrication was demonstrated by directly depositing Yb^{3+}- and Ce^{3+}-codoped $CsPbCl_{1.5}Br_{1.5}$ nanocrystals on the surface of commercial single-crystal silicon solar cells [35]. When irradiated under simulated AM1.5G sunlight with a 400-nm short-pass filter, the photoelectric conversion efficiency (PCE) increased from 18.1% to 21.5% after integration with a 230-nm-thick down converter (Fig. 14). Similar enhancement in PCE

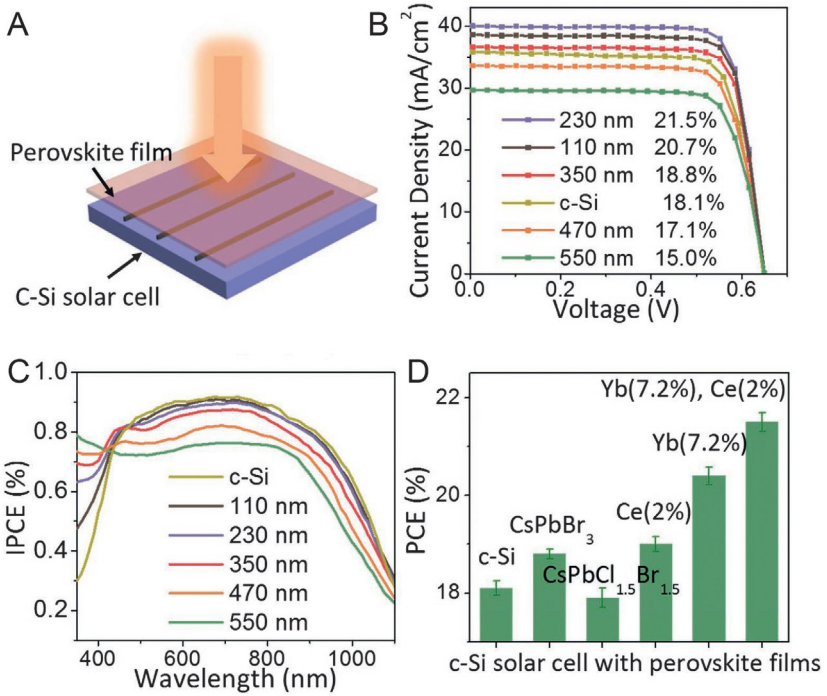

FIG. 14 (A) Schematic of crystalline-silicon solar cells integrated with a quantum-cutting film comprising Yb^{3+}-doped perovskites. (B) *I-V* curves of silicon solar cells coated with perovskite films of different thicknesses, recorded at a scan speed of $0.1\,V\,s^{-1}$. (C) IPCE curves of integrated silicon solar cells. (D) PCE of integrated silicon solar cells. *Adapted with permission from D. Zhou, D. Liu, G. Pan, X. Chen, D. Li, W. Xu, X. Bai, H. Song, Cerium and ytterbium codoped halide perovskite quantum dots: a novel and efficient downconverter for improving the performance of silicon solar cells, Adv. Mater. 29 (2017) 1704149, 10.1002/adma.201704149* © 2017 John Wiley and Sons.

was observed in $CuIn_{1-x}Ga_xSe_2$ (CIGS) solar cells in combination with $CsPbClBr_2$ nanocrystals doped with Yb^{3+}, Pr^{3+}, and Ce^{3+} ions [41]. Practical demonstration on mobile phone charging showed that the use of integrated solar cells shortened full charging by 30 min. These studies suggest a positive correlation between the quantum yields of quantum cutters and the PCE of solar photovoltaics.

Apart from lab-based demonstration, the practical performance of quantum cutter-paired solar cells can be predicted by theoretical modeling with realistic parameters such as actual hourly incident solar photon flux [62,63]. The modeling allows the identification of key factors determining the performance of integrated photovoltaic devices. These factors include the UV/blue absorption capacity of a given quantum cutter, quantum cutting efficiency, optical coupling between the quantum cutter and photovoltaics, and

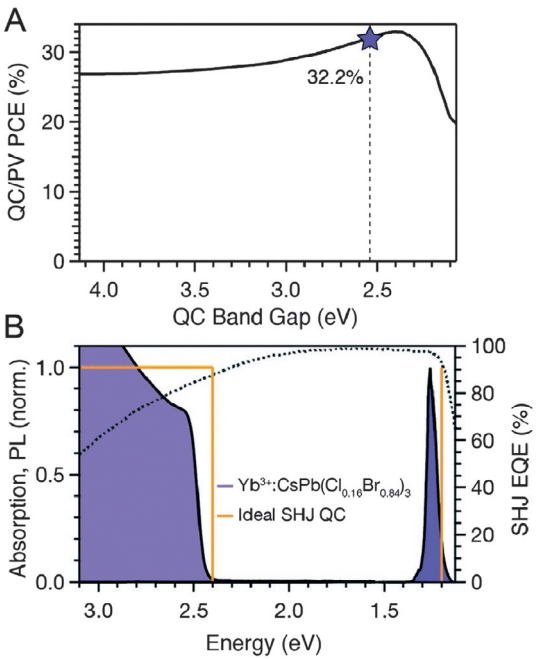

FIG. 15 (A) Detailed balance PCE of a Si heterojunction solar cell paired with a perfect quantum cutter. The star indicates a PCE of 32.2% achieved using a $CsPb(Cl_{1-x}Br_x)_3$:Yb quantum cutter with an optimized bandgap. (B) Absorption and photoluminescence spectra of an ideal quantum-cutting layer and a $CsPb(Cl_{0.16}Br_{0.84})_3$ layer. The dashed curve denotes the EQE of the Si heterojunction solar cell. *Adapted with permission from M.J. Crane, D.M. Kroupa, D.R. Gamelin, Detailed-balance analysis of Yb^{3+}:$CsPb(Cl_{1-x}Br_x)_3$ quantum-cutting layers for high-efficiency photovoltaics under real-world conditions, Energ. Environ. Sci. 12 (2019) 2486–2495, 10.1039/c9ee01493d* © 2019 Royal Society of Chemistry.

reflection/absorption losses. Simulations show that Yb^{3+}-doped perovskites can substantially improve the performance of solar cells based on Si heterojunction, CIGS, and multi-crystalline-Si [62]. When coupled to $CsPb(Cl_{0.16}Br_{0.84})_3$, the Si heterojunction yields the largest enhancement in PCE. The experimental absorption and photoluminescence spectra of $CsPb(Cl_{0.16}Br_{0.84})_3$ quantum cutters are close to those of an ideal quantum cutting layer (Fig. 15). The subtle interplays between the quantum cutting yield, the quantum cutter-photovoltaic optical coupling, and the bandgaps of quantum cutters and photovoltaic materials largely determine ultimate device performance. A customized design of Yb^{3+}-doped quantum cutters is required for specific photovoltaic solar cells to maximize device performance. It is worth mentioning that the power saturation of quantum cutting at realistic conditions should be less prominent because the photon flux of sunlight is less than AM1.5G. Simulations show that efficiency gain can still be achieved at different geographic locations under different spectral irradiances.

For device integration, the relative position between the quantum cutting layer and the solar cell module also affects device performance [63]. For example, incorporation of quantum-cutting layer between glass and encapsulation layer enables a power gain of 16.3% for silicon heterojunction modules, which is higher than achievable by directly placing the quantum cutting layer onto modules (Fig. 16). The power gain is mainly attributed to absorption of UV/blue photons by the quantum cutting layer without encapsulant interference. Given the isotropic nature of down-converted emission, the performance of integrated solar cells could be further enhanced by directing converted photons toward photovoltaic materials.

3.2 Luminescent solar concentrators (LSCs)

The basic working principle of LSCs involves light harvesting over a large area, photon conversion into emission, and confining of emitted photons into a small output area through internal reflections (Fig. 17) [64]. To optimize LSCs performance, four essential criteria must be met (i) large absorption cross-sections of luminescent materials, (ii) high photon conversion efficiency, (iii) minimal energy loss due to reabsorption, and (iv) high trapping efficiency of the waveguide. Conventional LSCs adopt organic dyes and colloidal quantum dots as luminophores [65,66]. However, further enhancement

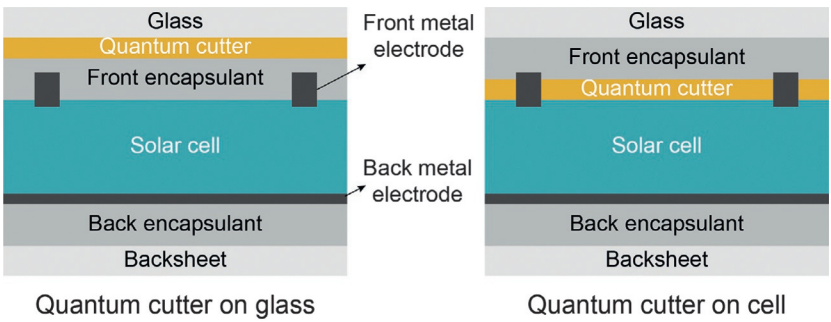

FIG. 16 Schematics of the relative position between a quantum-cutting layer and a solar cell.

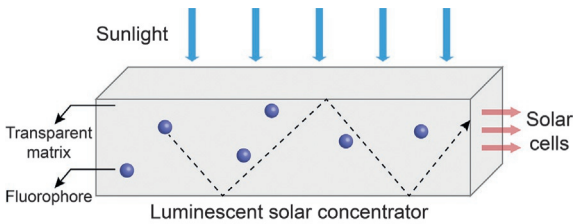

FIG. 17 Working principle of a luminescent solar concentrator.

in internal optical efficiencies of these LSCs is significantly limited by the reabsorption loss of emitted photons because these luminophores feature small Stokes shifts.

Recent studies demonstrate that prototype LSCs based on perovskite nanocrystals offer high absorption cross-sections, high quantum yields, and large Stokes shifts up to 1.5 eV [67]. Lanthanide incorporation can further expand the luminescence spectrum, enhance quantum yield, and enlarge the Stokes shift of perovskites, making them compelling for LSCs application [32]. In particular, Yb^{3+}-doped perovskites excel in both quantum yield (~170%) and Stokes shift (~2.05 eV) [39], promising as LSCs for NIR emission. For example, by embedding Yb^{3+}-doped $CsPbCl_3$ nanocrystals into a poly(methyl methacrylate) matrix, the fabricated LSC achieved an internal optical efficiency of 118%, twofold higher than that of LSCs comprising Mn^{2+}-doped quantum dots [68]. Notably, external optical efficiency exceeded 10% by increasing the solar absorbance of $CsPbCl_xBr_{3-x}$ nanocrystals via composition engineering. The most intriguing feature was that the performance of large-scale LSC devices retained over 100 cm^2, attributable to near-zero self-absorption loss of emitted NIR photons.

Another study demonstrated that codoping of $CsPbCl_3$:Mn^{2+} nanocrystals with Yb^{3+} ions enhances the operation performance of LSC devices (Fig. 18) [47]. For a $CsPbCl_3$:Mn/Yb-based LSC at a G-factor of 3.0, internal and external optical efficiencies increased 3.1- and 2.1-fold, respectively, compared with $CsPbCl_3$:Mn-based LSCs. A monolithic bilayer LSC containing a top-layer of $CsPb(Cl_{0.25}Br_{0.75})_3$:Yb nanocrystals and a bottom-layer of $CuInS_2$/ZnS nanocrystals achieved a 19% performance enhancement compared with $CuInS_2$/ZnS-based LSCs [69]. These emerging LSCs could boost photon-to-electricity conversion for many types of solar cells.

3.3 Light-emitting diodes

Emission modulation through lanthanide doping has opened another avenue toward perovskite-based light-emitting diodes. This was exemplified in Nd^{3+}/Cl^--codoped $CsPbBr_3$ nanocrystals in which dual doping enhanced excitonic emission with a spectral peak of 478 nm [70]. Despite the decrease in quantum yield from 97% in solution to 55% in the solid state, these Nd^{3+}/Cl^--codoped $CsPbBr_3$ nanocrystals enabled the fabrication of blue LEDs with 2.7% external quantum efficiency, a substantial enhancement compared with $CsPbBr_3$-based blue LEDs (0.07%) [71]. In addition to increasing host-exciton emission, incorporation of Ce^{3+}-Mn^{2+} pairs into $CsPbCl_{1.8}Br_{1.2}$ nanocrystals could generate blue, green, and red emission, making them suitable for white LEDs (Fig. 19) [72]. By way of illustration, color modulation of Sm^{3+}-doped $CsPbCl_3$ nanocrystals was achieved by varying the Sm^{3+} doping concentration that changed the luminescence ratio between exciton emission and host-sensitized Sm^{3+} emission [49]. Integration of a $CsPbCl_3$:

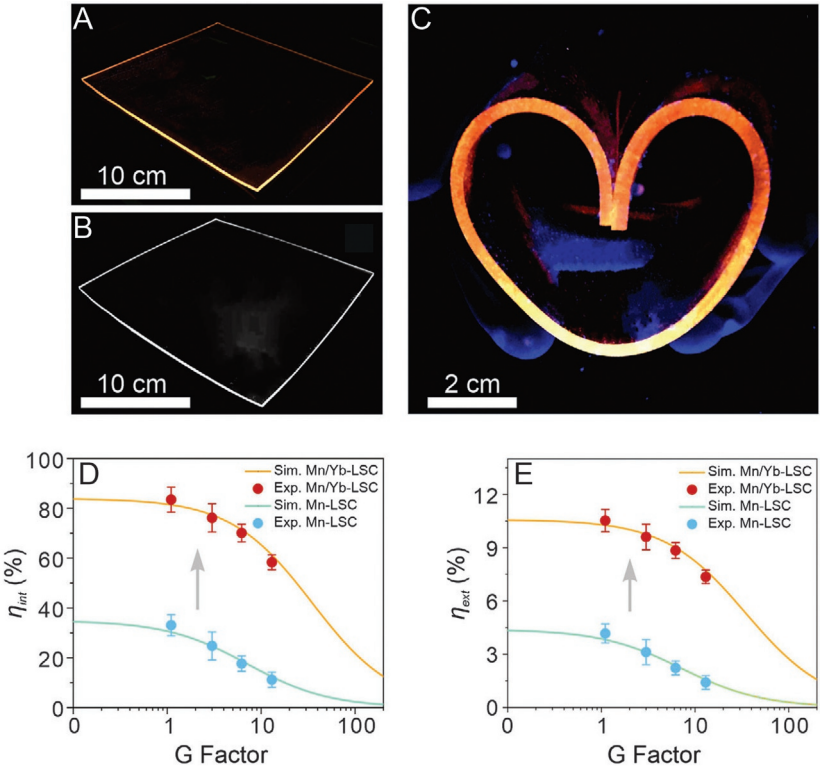

FIG. 18 (A and B) Photographs of a $CsPbCl_3$:Mn/Yb-based LSC upon 365-nm illumination, taken by a digital camera and a NIR camera (equipped with an 800-nm long-pass filter), respectively. (C) Photograph of the bent LSC upon 365-nm illumination, taken by a digital camera. (D and E) Internal optical efficiency (η_{int}) and external optical efficiency (η_{ext}) of $CsPbCl_3$:Mn- and $CsPbCl_3$:Mn/Yb-based LSCs under sunlight illumination, respectively. *Adapted with permission from T. Cai, J. Wang, W. Li, K. Hills-Kimball, H. Yang, Y. Nagaoka, Y. Yuan, R. Zia, O. Chen, Mn^{2+}/Yb^{3+} codoped $CsPbCl_3$ perovskite nanocrystals with triple-wavelength emission for luminescent solar concentrators, Adv. Sci. 7 (2020) 2001317, 10.1002/advs.202001317* © 2020 John Wiley and Sons.

Sm-based luminescent layer with charge carrier transport layers afforded white LEDs with CIE chromaticity coordinates of (0.32, 0.31) and a high color rendering index of 93.

Lanthanide-doped perovskites are useful in enhancing the responsivity of silicon photodetectors to UV radiation [73]. They can also boost the performance of photonic devices in 1.5-μm telecommunication wavelength [45], while monitoring temperature changes over a wide range with high sensitivity [74]. These emerging perovskite nanocrystals may find potential applications in bioimaging if their toxicity and stability issues can be resolved.

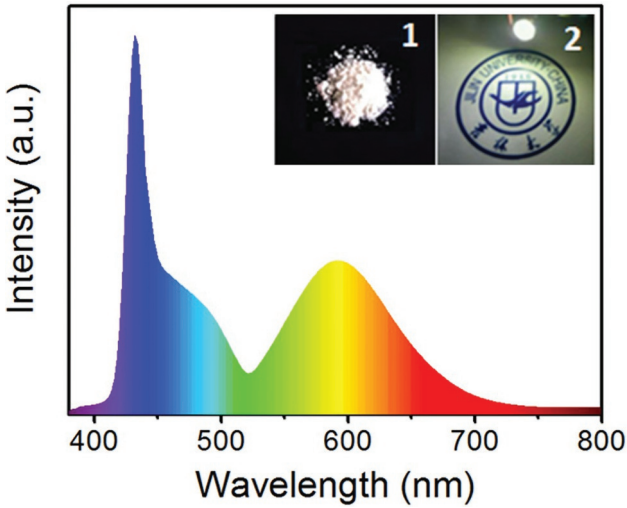

FIG. 19 Photoluminescence spectra of $CsPbCl_{1.8}Br_{1.2}$:Mn(9.1%)/Ce(2.7%) phosphor powder. Inset 1 is a photograph of the phosphor powder with polystyrene, and inset 2 is a photograph of the fabricated WLED operated at 3.0 V. *Adapted with permission from G. Pan, X. Bai, W. Xu, X. Chen, D. Zhou, J. Zhu, H. Shao, Y. Zhai, B. Dong, L. Xu, H. Song, Impurity ions codoped cesium lead halide perovskite nanocrystals with bright white light emission toward ultraviolet–white light-emitting diode, ACS Appl. Mater. Interfaces 10 (2018) 39040–39048, 10.1021/acsami.8b14275* © 2018 American Chemical Society.

4 Outlook

The interplay between perovskite hosts and lanthanide dopants empowers their hybrid composites with tunable luminescence profiles, increased quantum yields, and enhanced chemical stability for a broad range of applications, particularly in optoelectronics. Despite rapid progress, several challenges need to be addressed before device design proceeds. The first challenge is the mechanistic understanding of host sensitization. Previous literature suggests that nonradiative resonance energy transfer from the perovskite hosts to lanthanide ions occurs through a dipole-dipole coupling or an electron exchange mechanism. Consequently, the rate of energy transfer largely depends on the distance and spectral overlap between the hosts and dopants. However, experimental evidence in semiconducting CdSe and ZnS nanoparticles shows that the relative location of lanthanide energy levels with reference to host conduction and valence band edges can better predict nanocrystal optical properties than the spectral overlap [75]. This suggests a charge-trapping-mediated sensitization mechanism, which contradicts with the Förster or Dexter mechanism proposed in lanthanide-doped perovskite materials. Additionally, DFT calculation on $CsPbBr_3$:Ln^{3+} materials reveals that electrons at occupied

4*f* levels can be excited to host conduction bands upon irradiation, resulting in donor-like ionization [34]. The coexistence of ionization transition and band-edge transition may complicate the analysis of photophysical dynamics.

The second challenge is to unravel quantum cutting mechanisms. Although spectroscopic characterization suggests that doping-induced shallow traps are responsible for extraction of excitonic energy and its concurrent transfer to two Yb^{3+} ions, DFT calculations show that Pb^{2+} vacancies are most likely formed upon lanthanide doping and do not introduce shallow impurity states under the conduction band minimum of perovskite hosts. As such, identification of structural imperfection in both bulk and nanocrystalline materials deserves further research effort [76]. Identification of higher-lying excited states of Yb^{3+} in perovskite materials is also required to validate Auger-type cross-relaxation between host excitons and Yb^{3+} in its $^2F_{5/2}$ excited state [52]. Moreover, instead of simulations, photovoltaics and luminescent solar concentrators involving lanthanide-based quantum cutters must benchmark with commercial systems.

Another challenge that hinders the practical application of lanthanide-doped perovskites lies in their low resistance against heat, moisture, and photoirradiation. Laboratory tests on the long-term stability of $CsPbClBr_2$: Ce/Yb/Pr nanocrystal-based solar cells showed that the perovskite nanocrystals decomposed after 60-day under ambient conditions, resulting in an abrupt drop in PCE [41]. Surface passivation and encapsulation may enhance the stability of perovskite nanocrystals [77,78]. Zero-dimensional Cs_4PbX_6 ($X = Cl^-$, Br^-, or I^-) perovskites featuring high thermal and chemical stabilities could be used as alternative sensitizers [79]. For example, the outdoor lifetime of Cs_4PbBr_6-based solar concentrators was predicted to last over 7 months under 30 mW/cm^2 light exposure [80]. However, high levels of toxicity remain a concern for their widespread applications. The most straightforward solution is to replace lead with less toxic or nontoxic elements. Successful incorporation of lanthanide ions into lead-free inorganic halide perovskites has been extensively demonstrated [81–85]. Moreover, uneven distributions of lanthanide ions in lead-free double perovskites allow cross relaxation between Ln^{3+} ions to be controlled, enriching emission colors [86]. However, these lead-free perovskites exhibit much lower photoluminescence quantum yields than lead-containing perovskites.

Acknowledgments

This work is supported by NUS NANONASH Programme (NUHSRO/2020/002/NanoNash/LOA; R143000B43114), Agency for Science, Technology and Research (A*STAR) (Grant NO. A1983c0038), and National Research Foundation, Prime Minister's Office, Singapore under the NRF Investigatorship program (award no. NRF-NRFI05-2019-0003).

References

[1] J.C.G. Bünzli, C. Piguet, Taking advantage of luminescent lanthanide ions, Chem. Soc. Rev. 34 (2005) 1048–1077, https://doi.org/10.1039/b406082m.

[2] J. Xu, A. Gulzar, P. Yang, H. Bi, D. Yang, S. Gai, F. He, J. Lin, B. Xing, D. Jin, Recent advances in near-infrared emitting lanthanide-doped nanoconstructs: mechanism, design and application for bioimaging, Coord. Chem. Rev. 381 (2019) 104–134, https://doi.org/10.1016/j.ccr.2018.11.014.

[3] K.L. Bray, Luminescent materials by G. Blasse (University of Utrecht, The Netherlands) and B. C. Grabmaier (Siemens Research Laboratories), Springer, New York, 1994, 232 pp. $49.95. ISBN 0-387-58109-0, J. Am. Chem. Soc. 42 (1996) 10340, https://doi.org/10.1021/ja965667t.

[4] G.K. Liu, B. Jacquier, Spectroscopic Properties of Rare Earths in Optical Materials, Springer, Berlin, 2005.

[5] H. Zhang, Z.H. Chen, X. Liu, F. Zhang, A mini-review on recent progress of new sensitizers for luminescence of lanthanide doped nanomaterials, Nano Res. 13 (2020) 1795–1809, https://doi.org/10.1007/s12274-020-2661-8.

[6] R. Marin, D. Jaque, A. Benayas, Switching to the brighter lane: pathways to boost the absorption of lanthanide-doped nanoparticles, Nanoscale Horiz. 6 (2021) 209–230, https://doi.org/10.1039/d0nh00627k.

[7] G. Bao, S. Wen, G. Lin, J. Yuan, J. Lin, K.L. Wong, J.C.G. Bünzli, D. Jin, Learning from lanthanide complexes: the development of dye-lanthanide nanoparticles and their biomedical applications, Coord. Chem. Rev. 429 (2021) 213642. https://doi.org/10.1016/j.ccr.2020.213642.

[8] W. Luo, Y. Liu, X. Chen, Lanthanide-doped semiconductor nanocrystals: electronic structures and optical properties, Sci. China Mater. 58 (2015) 819–850, https://doi.org/10.1007/s40843-015-0091-9.

[9] R. Marin, D. Jaque, Doping lanthanide ions in colloidal semiconductor nanocrystals for brighter photoluminescence, Chem. Rev. 121 (2021) 1425–1462, https://doi.org/10.1021/acs.chemrev.0c00692.

[10] D.J. Garfield, N.J. Borys, S.M. Hamed, N.A. Torquato, C.A. Tajon, B. Tian, B. Shevitski, E.S. Barnard, Y.D. Suh, S. Aloni, J.B. Neaton, E.M. Chan, B.E. Cohen, P.J. Schuck, Enrichment of molecular antenna triplets amplifies upconverting nanoparticle emission, Nat. Photonics 12 (2018) 402–407, https://doi.org/10.1038/s41566-018-0156-x.

[11] S. Han, R. Deng, Q. Gu, L. Ni, U. Huynh, J. Zhang, Z. Yi, B. Zhao, H. Tamura, A. Pershin, H. Xu, Z. Huang, S. Ahmad, M. Abdi-Jalebi, A. Sadhanala, M.L. Tang, A. Bakulin, D. Beljonne, X. Liu, A. Rao, Lanthanide-doped inorganic nanoparticles turn molecular triplet excitons bright, Nature 587 (2020) 594–599, https://doi.org/10.1038/s41586-020-2932-2.

[12] L. Jing, S.V. Kershaw, Y. Li, X. Huang, Y. Li, A.L. Rogach, M. Gao, Aqueous based semiconductor nanocrystals, Chem. Rev. 116 (2016) 10623–10730, https://doi.org/10.1021/acs.chemrev.6b00041.

[13] A.J. Kenyon, Recent developments in rare-earth doped materials for optoelectronics, Prog. Quantum Electron. 26 (2002) 225–284, https://doi.org/10.1016/S0079-6727(02)00014-9.

[14] A.A. Bol, R. Van Beek, A. Meijerink, On the incorporation of trivalent rare earth ions in II-VI semiconductor nanocrystals, Chem. Mater. 14 (2002) 1121–1126, https://doi.org/10.1021/cm011195s.

[15] L. Protesescu, S. Yakunin, M.I. Bodnarchuk, F. Krieg, R. Caputo, C.H. Hendon, R.X. Yang, A. Walsh, M.V. Kovalenko, Nanocrystals of cesium lead halide perovskites ($CsPbX_3$, X = cl, Br, and I): novel optoelectronic materials showing bright emission with wide color gamut, Nano Lett. 15 (2015) 3692–3696, https://doi.org/10.1021/nl5048779.

[16] G. Nedelcu, L. Protesescu, S. Yakunin, M.I. Bodnarchuk, M.J. Grotevent, M.V. Kovalenko, Fast anion-exchange in highly luminescent nanocrystals of cesium lead halide perovskites ($CsPbX_3$, X = Cl, Br, I), Nano Lett. 15 (2015) 5635–5640, https://doi.org/10.1021/acs.nanolett.5b02404.

[17] Q.A. Akkerman, V. D'Innocenzo, S. Accornero, A. Scarpellini, A. Petrozza, M. Prato, L. Manna, Tuning the optical properties of cesium lead halide perovskite nanocrystals by anion exchange reactions, J. Am. Chem. Soc. 137 (2015) 10276–10281, https://doi.org/10.1021/jacs.5b05602.

[18] S. Sun, D. Yuan, Y. Xu, A. Wang, Z. Deng, Ligand-mediated synthesis of shape-controlled cesium lead halide perovskite nanocrystals via reprecipitation process at room temperature, ACS Nano 10 (2016) 3648–3657, https://doi.org/10.1021/acsnano.5b08193.

[19] Z.J. Yong, S.Q. Guo, J.P. Ma, J.Y. Zhang, Z.Y. Li, Y.M. Chen, B. Bin Zhang, Y. Zhou, J. Shu, J.L. Gu, L.R. Zheng, O.M. Bakr, H.T. Sun, Doping-enhanced short-range order of perovskite nanocrystals for near-unity violet luminescence quantum yield, J. Am. Chem. Soc. 140 (2018) 9942–9951, https://doi.org/10.1021/jacs.8b04763.

[20] W.J. Mir, T. Sheikh, H. Arfin, Z. Xia, A. Nag, Lanthanide doping in metal halide perovskite nanocrystals: spectral shifting, quantum cutting and optoelectronic applications, NPG Asia Mater. 12 (2020) 9, https://doi.org/10.1038/s41427-019-0192-0.

[21] S.M. Ferro, M. Wobben, B. Ehrler, Rare-earth quantum cutting in metal halide perovskites—a review, Mater. Horizons 8 (2021) 1072–1083, https://doi.org/10.1039/d0mh01470b.

[22] W. Zheng, P. Huang, Z. Gong, D. Tu, J. Xu, Q. Zou, R. Li, W. You, J.C.G. Bünzli, X. Chen, Near-infrared-triggered photon upconversion tuning in all-inorganic cesium lead halide perovskite quantum dots, Nat. Commun. 9 (2018) 3462, https://doi.org/10.1038/s41467-018-05947-2.

[23] D.M. Kroupa, J.Y. Roh, T.J. Milstein, S.E. Creutz, D.R. Gamelin, Quantum-cutting ytterbium-doped $CsPb(Cl_{1-x}Br_x)_3$ perovskite thin films with photoluminescence quantum yields over 190%, ACS Energy Lett. 3 (2018) 2390–2395, https://doi.org/10.1021/acsenergylett.8b01528.

[24] S.E. Creutz, R. Fainblat, Y. Kim, M.C. De Siena, D.R. Gamelin, A selective cation exchange strategy for the synthesis of colloidal Yb^{3+}-doped chalcogenide nanocrystals with strong broadband visible absorption and long-lived near-infrared emission, J. Am. Chem. Soc. 139 (2017) 11814–11824, https://doi.org/10.1021/jacs.7b04938.

[25] R. Martín-Rodríguez, R. Geitenbeek, A. Meijerink, Incorporation and luminescence of Yb^{3+} in CdSe nanocrystals, J. Am. Chem. Soc. 135 (2013) 13668–13671, https://doi.org/10.1021/ja4077414.

[26] B.W. Wessels, Rare-earth doped semiconductors for linear and nonlinear optical applications, in: B. Di Bartolo (Ed.), Nonlinear Spectroscopy of Solids, NATO ASI Series (Series B: Physics), Springer, Boston, MA, 1994, p. 583, https://doi.org/10.1007/978-1-4899-1190-2_27.

[27] Y. Liu, W. Luo, H. Zhu, X. Chen, Optical spectroscopy of lanthanides doped in wide band-gap semiconductor nanocrystals, JOL 131 (2011) 415–422, https://doi.org/10.1016/j.jlumin.2010.07.018.

[28] J. Kang, L.W. Wang, High defect tolerance in lead halide perovskite $CsPbBr_3$, J. Phys. Chem. Lett. 8 (2017) 489–493, https://doi.org/10.1021/acs.jpclett.6b02800.

[29] V.M. Goldschmidt, Die Gesetze der Krystallochemie, Naturwissenschaften 14 (1926) 477–485, https://doi.org/10.1007/BF01507527.

[30] G. Kieslich, S. Sun, A.K. Cheetham, Solid-state principles applied to organic–inorganic perovskites: new tricks for an old dog, Chem. Sci. 5 (2014) 4712–4715, https://doi.org/10.1039/c4sc02211d.

[31] W. Travis, E.N.K. Glover, H. Bronstein, D.O. Scanlon, R.G. Palgrave, On the application of the tolerance factor to inorganic and hybrid halide perovskites: a revised system, Chem. Sci. 7 (2016) 4548–4556, https://doi.org/10.1039/c5sc04845a.

[32] G. Pan, X. Bai, D. Yang, X. Chen, P. Jing, S. Qu, L. Zhang, D. Zhou, J. Zhu, W. Xu, B. Dong, H. Song, Doping lanthanide into perovskite nanocrystals: highly improved and expanded optical properties, Nano Lett. 17 (2017) 8005–8011, https://doi.org/10.1021/acs.nanolett.7b04575.

[33] J.P. Ma, Y.M. Chen, L.M. Zhang, S.Q. Guo, J.D. Liu, H. Li, B.J. Ye, Z.Y. Li, Y. Zhou, B. Bin Zhang, O.M. Bakr, J.Y. Zhang, H.T. Sun, Insights into the local structure of dopants, doping efficiency, and luminescence properties of lanthanide-doped $CsPbCl_3$ perovskite nanocrystals, J. Mater. Chem. C. 7 (2019) 3037–3048, https://doi.org/10.1039/c9tc00237e.

[34] L. He, J. Meng, J. Feng, X. Liu, H. Zhang, Unveiling the mechanism of rare earth doping to optimize the optical performance of the $CsPbBr_3$ perovskite, Inorg. Chem. Front. 7 (2020) 4669–4676, https://doi.org/10.1039/d0qi01077d.

[35] D. Zhou, D. Liu, G. Pan, X. Chen, D. Li, W. Xu, X. Bai, H. Song, Cerium and ytterbium codoped halide perovskite quantum dots: a novel and efficient downconverter for improving the performance of silicon solar cells, Adv. Mater. 29 (2017) 1704149, https://doi.org/10.1002/adma.201704149.

[36] Q. Hu, Z. Li, Z. Tan, H. Song, C. Ge, G. Niu, J. Han, J. Tang, Rare earth ion-doped $CsPbBr_3$ nanocrystals, Adv. Opt. Mater. 6 (2018) 1700864, https://doi.org/10.1002/adom.201700864.

[37] D. Parobek, B.J. Roman, Y. Dong, H. Jin, E. Lee, M. Sheldon, D.H. Son, Exciton-to-dopant energy transfer in Mn-doped cesium lead halide perovskite nanocrystals, Nano Lett. 16 (2016) 7376–7380, https://doi.org/10.1021/acs.nanolett.6b02772.

[38] D. Rossi, D. Parobek, Y. Dong, D.H. Son, Dynamics of exciton-Mn energy transfer in Mn-doped $CsPbCl_3$ perovskite nanocrystals, J. Phys. Chem. C 121 (2017) 17143–17149, https://doi.org/10.1021/acs.jpcc.7b06182.

[39] T.J. Milstein, D.M. Kroupa, D.R. Gamelin, Picosecond quantum cutting generates photoluminescence quantum yields over 100% in ytterbium-doped $CsPbCl_3$ nanocrystals, Nano Lett. 18 (2018) 3792–3799, https://doi.org/10.1021/acs.nanolett.8b01066.

[40] M.J. Crane, D.M. Kroupa, J.Y. Roh, R.T. Anderson, M.D. Smith, D.R. Gamelin, Single-source vapor deposition of quantum-cutting Yb^{3+}:$CsPb(Cl_{1-x}Br_x)_3$ and other complex metal-halide perovskites, ACS Appl. Energy Mater. 2 (2019) 4560–4565, https://doi.org/10.1021/acsaem.9b00910.

[41] D. Zhou, R. Sun, W. Xu, N. Ding, D. Li, X. Chen, G. Pan, X. Bai, H. Song, Impact of host composition, codoping, or tridoping on quantum-cutting emission of ytterbium in halide perovskite quantum dots and solar cell applications, Nano Lett. 19 (2019) 6904–6913, https://doi.org/10.1021/acs.nanolett.9b02139.

[42] X. Huang, S. Han, W. Huang, X. Liu, Enhancing solar cell efficiency: the search for luminescent materials as spectral converters, Chem. Soc. Rev. 42 (2013) 173–201, https://doi.org/10.1039/c2cs35288e.

[43] J.Y.D. Roh, M.D. Smith, M.J. Crane, D. Biner, T.J. Milstein, K.W. Krämer, D.R. Gamelin, Yb^{3+} speciation and energy-transfer dynamics in quantum-cutting Yb^{3+}-doped $CsPbCl_3$ perovskite

nanocrystals and single crystals, Phys. Rev. Mater. 4 (2020) 105405. https://doi.org/10.1103/PhysRevMaterials.4.105405.

[44] X. Zhang, Y. Zhang, X. Zhang, W. Yin, Y. Wang, H. Wang, M. Lu, Z. Li, Z. Gu, W.W. Yu, Yb^{3+} and Yb^{3+}/Er^{3+} doping for near-infrared emission and improved stability of $CsPbCl_3$ nanocrystals, J. Mater. Chem. C. 6 (2018) 10101–10105, https://doi.org/10.1039/c8tc03957g.

[45] M. Zeng, F. Artizzu, J. Liu, S. Singh, F. Locardi, D. Mara, Z. Hens, R., Van Deun, boosting the Er^{3+} 1.5 μm luminescence in $CsPbCl_3$ perovskite nanocrystals for photonic devices operating at telecommunication wavelengths, ACS Appl, Nano Mater. 3 (2020) 4699–4707, https://doi.org/10.1021/acsanm.0c00701.

[46] Y. Zhu, G. Pan, L. Shao, G. Yang, X. Xu, J. Zhao, Y. Mao, Effective infrared emission of erbium ions doped inorganic lead halide perovskite quantum dots by sensitization of ytterbium ions, J. Alloys Compd. 835 (2020) 155390. https://doi.org/10.1016/j.jallcom.2020.155390.

[47] T. Cai, J. Wang, W. Li, K. Hills-Kimball, H. Yang, Y. Nagaoka, Y. Yuan, R. Zia, O. Chen, Mn^{2+}/Yb^{3+} codoped $CsPbCl_3$ perovskite nanocrystals with triple-wavelength emission for luminescent solar concentrators, Adv. Sci. 7 (2020) 2001317, https://doi.org/10.1002/advs.202001317.

[48] Y. Zhai, X. Bai, G. Pan, J. Zhu, H. Shao, B. Dong, L. Xu, H. Song, Effective blue-violet photoluminescence through lanthanum and fluorine ions co-doping for $CsPbCl_3$ perovskite quantum dots, Nanoscale 11 (2019) 2484–2491, https://doi.org/10.1039/c8nr09794a.

[49] R. Sun, P. Lu, D. Zhou, W. Xu, N. Ding, H. Shao, Y. Zhang, D. Li, N. Wang, X. Zhuang, B. Dong, X. Bai, H. Song, Samarium-doped metal halide perovskite nanocrystals for single-component electroluminescent white light-emitting diodes, ACS Energy Lett. 5 (2020) 2131–2139, https://doi.org/10.1021/acsenergylett.0c00931.

[50] Q. Li, Y. Liu, P. Chen, J. Hou, Y. Sun, G. Zhao, N. Zhang, J. Zou, J. Xu, Y. Fang, N. Dai, Excitonic luminescence engineering in tervalent-europium-doped cesium lead halide perovskite nanocrystals and their temperature-dependent energy transfer emission properties, J. Phys. Chem. C 122 (2018) 29044–29050, https://doi.org/10.1021/acs.jpcc.8b10107.

[51] T.J. Milstein, K.T. Kluherz, D.M. Kroupa, C.S. Erickson, J.J. De Yoreo, D.R. Gamelin, Anion exchange and the quantum-cutting energy threshold in ytterbium-doped $CsPb(Cl_{1-x}Br_x)_3$ perovskite nanocrystals, Nano Lett. 19 (2019) 1931–1937, https://doi.org/10.1021/acs.nanolett.8b05104.

[52] C.S. Erickson, M.J. Crane, T.J. Milstein, D.R. Gamelin, Photoluminescence saturation in quantum-cutting Yb^{3+}-doped $CsPb(Cl_{1-x}Br_x)_3$ perovskite nanocrystals: implications for solar downconversion, J. Phys. Chem. C 123 (2019) 12474–12484, https://doi.org/10.1021/acs.jpcc.9b01296.

[53] K. Watanabe, M. Koshimizu, T. Yanagida, Y. Fujimoto, K. Asai, Luminescence and scintillation properties of La- and La,Ag-doped $CsPbCl_3$ single crystals, Jpn. J. Appl. Phys. 55 (2016) 02BC20. https://doi.org/10.7567/JJAP.55.02BC20.

[54] L.M. Henling, G.L. McPherson, EPR spectra of magnetically coupled pairs of Gd^{3+} ions in crystals of $CsMgCl_3$, $CsMgBr_3$, and $CsCdBr_3$, Phys. Rev. B. 16 (1977) 4756, https://doi.org/10.1103/PhysRevB.16.4756.

[55] X. Li, S. Duan, H. Liu, G. Chen, Y. Luo, H. Ågren, Mechanism for the extremely efficient sensitization of Yb^{3+} luminescence in $CsPbCl_3$ nanocrystals, J. Phys. Chem. Lett. 10 (2019) 487–492, https://doi.org/10.1021/acs.jpclett.8b03406.

[56] J.P. Correa-Baena, M. Saliba, T. Buonassisi, M. Grätzel, A. Abate, W. Tress, A. Hagfeldt, Promises and challenges of perovskite solar cells, Science 358 (2017) 739–744, https://doi.org/10.1126/science.aam6323.

[57] R.E. Brandt, J.R. Poindexter, P. Gorai, R.C. Kurchin, R.L.Z. Hoye, L. Nienhaus, M.W.B. Wilson, J.A. Polizzotti, R. Sereika, R. Žaltauskas, L.C. Lee, J.L. Macmanus-Driscoll, M. Bawendi, V. Stevanović, T. Buonassisi, Searching for "defect-tolerant" photovoltaic materials: combined theoretical and experimental screening, Chem. Mater. 29 (2017) 4667–4674, https://doi.org/10.1021/acs.chemmater.6b05496.

[58] S. Mei, J. Zhou, H.T. Sun, Y. Cai, L.D. Sun, D. Jin, C.H. Yan, Networking state of ytterbium ions probing the origin of luminescence quenching and activation in nanocrystals, Adv. Sci. 8 (2021) 2003325, https://doi.org/10.1002/advs.202003325.

[59] Y. Wu, J. Xu, E.T. Poh, L. Liang, H. Liu, J.K.W. Yang, C.W. Qiu, R.A.L. Vallée, X. Liu, Upconversion superburst with sub-2 μs lifetime, Nat. Nanotechnol. 14 (2019) 1110–1115, https://doi.org/10.1038/s41565-019-0560-5.

[60] X. Qin, A.N. Carneiro Neto, R.L. Longo, Y. Wu, O.L. Malta, X. Liu, Surface plasmon-photon coupling in lanthanide-doped nanoparticles, J. Phys. Chem. Lett. 12 (2021) 1520–1541, https://doi.org/10.1021/acs.jpclett.0c03613.

[61] T. Trupke, M.A. Green, P. Würfel, Improving solar cell efficiencies by down-conversion of high-energy photons, J. Appl. Phys. 92 (2002) 1668, https://doi.org/10.1063/1.1492021.

[62] M.J. Crane, D.M. Kroupa, D.R. Gamelin, Detailed-balance analysis of Yb^{3+}: $CsPb(Cl_{1-x}Br_x)_3$ quantum-cutting layers for high-efficiency photovoltaics under real-world conditions, Energ. Environ. Sci. 12 (2019) 2486–2495, https://doi.org/10.1039/c9ee01493d.

[63] D.M. Kroupa, M.J. Crane, J.S. Silvia, D.R. Gamelin, Ray-tracing analysis of module-level power generation from quantum-cutting ytterbium-doped metal-halide perovskites, 47th IEEE Photovolt, Spec. Conf. 2020 (2020) 0868–0874, https://doi.org/10.1109/PVSC45281.2020.9300410.

[64] K. Jo, H.J. Kim, Review of the fundamental principles and performances on luminescent solar concentrators, Appl. Sci. Converg. Technol. 30 (2021) 14–20, https://doi.org/10.5757/ASCT.2021.30.1.14.

[65] Y. Zhao, G.A. Meek, B.G. Levine, R.R. Lunt, Near-infrared harvesting transparent luminescent solar concentrators, Adv. Opt. Mater. 2 (2014) 606–611, https://doi.org/10.1002/adom.201400103.

[66] F. Meinardi, S. Ehrenberg, L. Dhamo, F. Carulli, M. Mauri, F. Bruni, R. Simonutti, U. Kortshagen, S. Brovelli, Highly efficient luminescent solar concentrators based on earth-abundant indirect-bandgap silicon quantum dots, Nat. Photonics 11 (2017) 177–185, https://doi.org/10.1038/nphoton.2017.5.

[67] H. Zhao, Perovskite quantum dots based luminescent solar concentrators, in: Y. Zhou, Y. Wang (Eds.), Perovskite Quantum Dots, Springer Ser. Mater. Sci., Springer, Singapore, 2020, pp. 219–242, https://doi.org/10.1007/978-981-15-6637-0_8.

[68] K. Wu, H. Li, V.I. Klimov, Tandem luminescent solar concentrators based on engineered quantum dots, Nat. Photonics 12 (2018) 105–110, https://doi.org/10.1038/s41566-017-0070-7.

[69] T.A. Cohen, T.J. Milstein, D.M. Kroupa, J.D. Mackenzie, C.K. Luscombe, D.R. Gamelin, Quantum-cutting Yb^{3+}-doped perovskite nanocrystals for monolithic bilayer luminescent solar concentrators, J. Mater. Chem. A 7 (2019) 9279–9288, https://doi.org/10.1039/c9ta01261c.

[70] T. Chiba, J. Sato, S. Ishikawa, Y. Takahashi, H. Ebe, S. Sumikoshi, S. Ohisa, J. Kido, Neodymium chloride-doped perovskite nanocrystals for efficient blue light-emitting devices, ACS Appl. Mater. Interfaces 12 (2020) 53891–53898, https://doi.org/10.1021/acsami.0c11736.

[71] T. Fang, F. Zhang, S. Yuan, H. Zeng, J. Song, Recent advances and prospects toward blue perovskite materials and light-emitting diodes, InfoMat 1 (2019) 211–233, https://doi.org/10.1002/inf2.12019.

[72] G. Pan, X. Bai, W. Xu, X. Chen, D. Zhou, J. Zhu, H. Shao, Y. Zhai, B. Dong, L. Xu, H. Song, Impurity ions codoped cesium lead halide perovskite nanocrystals with bright white light emission toward ultraviolet–white light-emitting diode, ACS Appl. Mater. Interfaces 10 (2018) 39040–39048, https://doi.org/10.1021/acsami.8b14275.

[73] N. Ding, W. Xu, D. Zhou, Y. Ji, Y. Wang, R. Sun, X. Bai, J. Zhou, H. Song, Extremely efficient quantum-cutting Cr^{3+}, Ce^{3+}, Yb^{3+} tridoped perovskite quantum dots for highly enhancing the ultraviolet response of silicon photodetectors with external quantum efficiency exceeding 70%, Nano Energy 78 (2020) 105278. https://doi.org/10.1016/j.nanoen.2020.105278.

[74] Y. Zhang, J. Liu, H. Zhang, Q. He, X. Liang, W. Xiang, Ultra-stable Tb^{3+}:$CsPbI_3$ nanocrystal glasses for wide-range high-sensitivity optical temperature sensing, J. Eur. Ceram. Soc. 40 (2020) 6023–6030, https://doi.org/10.1016/j.jeurceramsoc.2020.07.016.

[75] G.H. Debnath, P. Mukherjee, D.H. Waldeck, Optimizing the key variables to generate host sensitized lanthanide doped semiconductor nanoparticle luminophores, J. Phys. Chem. C 124 (2020) 26495–26517, https://doi.org/10.1021/acs.jpcc.0c07548.

[76] L. Piveteau, M. Aebli, N. Yazdani, M. Millen, L. Korosec, F. Krieg, B.M. Benin, V. Morad, C. Piveteau, T. Shiroka, A. Comas-Vives, C. Copéret, A.M. Lindenberg, V. Wood, R. Verel, M.V. Kovalenko, Bulk and nanocrystalline cesium lead-halide perovskites as seen by halide magnetic resonance, ACS Cent. Sci. 6 (2020) 1138–1149, https://doi.org/10.1021/acscentsci.0c00587.

[77] W. Lv, L. Li, M. Xu, J. Hong, X. Tang, L. Xu, Y. Wu, R. Zhu, R. Chen, W. Huang, Improving the stability of metal halide perovskite quantum dots by encapsulation, Adv. Mater. 31 (2019) 1900682, https://doi.org/10.1002/adma.201900682.

[78] X. Wang, Z. Bao, Y.C. Chang, R.S. Liu, Perovskite quantum dots for application in high color gamut backlighting display of light-emitting diodes, ACS Energy Lett. 5 (2020) 3374–3396, https://doi.org/10.1021/acsenergylett.0c01860.

[79] O.F. Mohammed, Outstanding challenges of zero-dimensional perovskite materials, J. Phys. Chem. Lett. 10 (2019) 5886–5888, https://doi.org/10.1021/acs.jpclett.9b00175.

[80] Y. Liu, N. Li, R. Sun, W. Zheng, T. Liu, H. Li, Y. Chen, G. Liu, H. Zhao, H. Liu, Y. Zhang, Stable metal-halide perovskites for luminescent solar concentrators of real-device integration, Nano Energy 85 (2021) 105960. https://doi.org/10.1016/j.nanoen.2021.105960.

[81] S. Li, Q. Hu, J. Luo, T. Jin, J. Liu, J. Li, Z. Tan, Y. Han, Z. Zheng, T. Zhai, H. Song, L. Gao, G. Niu, J. Tang, Self-trapped exciton to dopant energy transfer in rare earth doped lead-free double perovskite, Adv. Opt. Mater. 7 (2019) 1901098, https://doi.org/10.1002/adom.201901098.

[82] W. Lee, S. Hong, S. Kim, Colloidal synthesis of lead-free silver–indium double-perovskite $Cs_2AgInCl_6$ nanocrystals and their doping with lanthanide ions, J. Phys. Chem. C 123 (2019) 2665–2672, https://doi.org/10.1021/acs.jpcc.8b12146.

[83] F. Schmitz, K. Guo, J. Horn, R. Sorrentino, G. Conforto, F. Lamberti, R. Brescia, F. Drago, M. Prato, Z. He, U. Giovanella, F. Cacialli, D. Schlettwein, D. Meggiolaro, T. Gatti, Lanthanide-induced photoluminescence in lead-free $Cs_2AgBiBr_6$ bulk perovskite: Insights from optical and theoretical investigations, J. Phys. Chem. Lett. 11 (2020) 8893–8900, https://doi.org/10.1021/acs.jpclett.0c02317.

[84] Y. Liu, M.S. Molokeev, Z. Xia, Lattice doping of lanthanide ions in $Cs_2AgInCl_6$ nanocrystals enabling tunable photoluminescence, Energy Mater. Adv. 2021 (2021) 2585274, https://doi.org/10.34133/2021/2585274.

[85] Y. Zhu, J. Zhu, H. Song, J. Huang, Z. Lu, G. Pan, Samarium doping improves luminescence efficiency of $Cs_3Bi_2Br_9$ perovskite quantum dots enabling efficient white light-emitting diodes, J. Rare Earths 39 (2021) 374–379, https://doi.org/10.1016/j.jre.2020.06.007.

[86] F. Piccinelli, I. Carrasco, C.-G. Ma, M. Bettinelli, Systematic analysis of the crystal chemistry and Eu^{3+} spectroscopy along the series of double perovskites Ca_2LnSbO_6 (ln = La, Eu, Gd, Lu, and Y), Inorg. Chem. 60 (2021) 8259–8266, https://doi.org/10.1021/acs.inorgchem.1c00932.